IEEE Access
Multidisciplinary | Rapid Review | Open Access Journal

Received January 28, 2019, accepted February 12, 2019, date of publication March 5, 2019, date of current version March 25, 2019.

Digital Object Identifier 10.1109/ACCESS.2019.2903204

Early Fault Diagnosis for Planetary Gearbox Based on Adaptive Parameter Optimized VMD and Singular Kurtosis Difference Spectrum

CHAOGE WANG, (Student Member, IEEE), HONGKUN LI, GANGJIN HUANG, AND JIAYU OU
School of Mechanical Engineering, Dalian University of Technology, Dalian 116024, China
Corresponding author: Hongkun Li (lihk@dlut.edu.cn)

This work was supported by the National Natural Science Foundation of China under Grant 51575075.

ABSTRACT Variational mode decomposition (VMD) is widely used in the condition monitoring and fault diagnosis of rotary machinery for its unique advantages. An adaptive parameter optimized VMD (APOVMD) is proposed in order to adaptively determine the suitable decomposed parameters and further enhance its performance. The traditional singular value decomposition (SVD) method cannot effectively select the reconstructed order, which often leads to unsatisfactory results for signal reconstruction. Thus, a singular kurtosis difference spectrum method is proposed to accurately determine the effective reconstructed order for signal noise reduction. In addition, because the fault signal of the planetary gearbox at the early fault stage is weak and susceptible to ambient noise and other signal interference, the fault feature information is difficult to extract. To address this issue, a novel method for early fault feature extraction of planetary gearbox based on APOVMD and singular kurtosis difference spectrum is proposed in this paper. First, the APOVMD is applied to decompose the planetary gearbox vibration signal into a series of band-limited intrinsic mode functions adaptively and non-recursively. Second, the sensitive component is selected from the IMFS according to the cosine similarity index. Third, the Hankel matrix is constructed for the sensitive component in the phase space and decomposed by SVD. Here, the effective reconstructed order is automatically selected by the singular kurtosis difference spectrum method for noise reduction. Finally, the Hilbert envelope spectrum analysis is carried out on the reconstructed signal, and the fault characteristic frequency information of planetary gearbox can be accurately extracted from the envelope spectrum to realize the fault identification and location. The results of simulation studies and actual experimental data analysis demonstrate that the proposed method has superior ability to extract the early weak fault characteristics of the planetary gearbox compared with the VMD-SVD and EEMD-SVD methods, and the validity and feasibility of the presented method are proved.

INDEX TERMS Planetary gearbox, adaptive parameter optimized VMD, singular kurtosis difference spectrum, cosine similarity, early fault diagnosis.

I. INTRODUCTION

Planetary gearboxes have the advantages of small size, large transmission ratio, strong bearing capacity, and high efficiency. Therefore, planetary gearboxes are widely used in helicopters, wind turbines, ships, heavy trucks, mining excavators and other large mechanical equipment [1]. The working environment of planetary gearboxes is commonly harsh. They operate under heavy load, fatigue and strong impact for a long time, which can easily lead to local faults such as pitting, cracking and broken teeth of the gear. Once a fault occurs to the planetary gearbox, it may lead to destroy the equipment and the whole power transmission system. Therefore, the research on incipient fault diagnosis of planetary gearbox can realize the early warning of equipment, and then formulate scientific maintenance methods to avoid catastrophic accidents [2], [3].

When a local fault occurs on the gear, the defect location will induce periodic and non-stationary impact vibration during the gear pair meshing [4]. Due to the influence of complex transmission path, fault vibration will be gradually weakened in the process of outward transmission.

The associate editor coordinating the review of this manuscript and approving it for publication was Chuan Li.

Moreover, the meshing vibrations of multiple pairs of gear in planetary gearbox are coupled with each other, which makes the vibration response signal obtained from the gearbox housing non-stationary and non-linear [5], [6]. Time-frequency analysis methods such as Wigner-Ville distribution (WVD) [7], short time Fourier transform (STFT) [8], and discrete wavelet transform (DWT) [9] are powerful tools for analyzing non-stationary and non-linear signals. However, these methods have their own limitations. The WVD has serious cross interference when it is used to analyze multi-component signals. The STFT has the disadvantage of fixed time-frequency resolution. The DWT needs to predetermine the wavelet basis function and the number of decomposition layers, which makes it lack of adaptability. Therefore, the non-adaptive signal processing method is difficult to achieve satisfactory results for the analysis of actual signals. Empirical mode decomposition (EMD) can adaptively decomposes the signal into a series of intrinsic mode functions according to the local scale features of the signal itself, thus revealing the internal nature of the signal [10]–[12]. However, EMD has the problems of over-envelope, under-envelope, endpoint effect and modal mixing. In order to explore a more suitable time-frequency analysis method, Simith [13] proposed the local mean decomposition (LMD) method, which overcomes the problems of over-envelope and under-envelope in EMD, and has the advantages of less endpoint effect and less iterations. However, LMD also has the problem of modal mixing. In order to suppress modal mixing, Huang and Wu [14] proposed the ensemble empirical mode decomposition (EEMD) method. Subsequently, Yang *et al.* [15] proposed the ensemble local mean decomposition (ELMD) method based on LMD and EEMD. However, as noise-aided algorithms, EEMD and ELMD will inevitably leave residual white noise in the decomposed signal. In addition, when the amount of white noise added is large, the average number of integration also needs to be increased, which results in taking more time to decompose the signal [16].

In order to overcome the shortcomings of the analysis method mentioned above, a new adaptive signal decomposition method, which is called Variational Mode Decomposition (VMD), is recently proposed by Dragomiretskiy and Zosso [17]. VMD is an entirely non-recursive signal decomposition algorithm, which transfers the signal decomposition process into the variational framework, and determines the frequency center and bandwidth of each component by searching for the optimal solution of the variational model [18], [19]. Due to the fact that VMD abandons the constraint of recursive decomposition, it can effectively avoid the mode mixing problem in EMD and LMD. Meanwhile, VMD can also effectively alleviate the shortcomings of EEMD and ELMD, and has high computational efficiency and good noise robustness [20]. Therefore, since VMD method was proposed, it has been widely used in the fields of fault diagnosis [21], signal processing [22], and image processing [23]. However, the superiority of VMD depends on the accuracy settings of decomposed mode number and penalty factor, which will lead to information loss or over decomposition and affect the result of feature extraction. In order to overcome the limitations of the VMD, an adaptive parameter optimization VMD (APOVMD) method is proposed in this paper, which can adaptively determine the most suitable decomposed parameters and improve the performance of VMD.

Because the early fault feature information of planetary gearbox is weak and seriously disturbed by background noise, therefore, only using a single VMD method is often not ideal. We try to combine it with other methods to achieve the purpose of feature extraction. Singular value decomposition (SVD), as a non-linear filtering method, can effectively eliminate the random noise components in the signal and obtain relatively pure fault signal [24]–[26]. However, the selection of reconstructed order will directly affect the quality of the noise reduction signal [27]. Previously, the reconstructed order was usually determined by the user's experience, which could not be automatically selected [28]. Then, some scholars put forward the method of singular value difference spectrum to determine the effective reconstruction order [29]. However, this method will miss some important information related to the fault when the fault signal is weak, and it is also difficult to achieve satisfactory results. Therefore, on the basis of traditional singular value decomposition, a singular value kurtosis difference spectrum method is proposed to accurately determine effective reconstructed order for signal noise reduction.

Based on the above analysis, a novel early fault feature extraction method based on APOVMD and singular value kurtosis difference spectrum is proposed in this paper. The simulation analysis and experimental verification of planetary gearbox will also be conducted to verify the effectiveness and superiority of the proposed method and compare with VMD-SVD method [30] and EEMD-SVD method [31], [32]. Hereafter, the remainder of this paper is organized as follows: Sections 2 introduce the theory of VMD and singular value difference, as well as the cosine similarity. In Section 3, the novel method adaptive parameter optimized VMD is presented in Section 3.1, the selection method singular kurtosis difference spectrum is given in Section 3.2, and the detailed implementation steps of the proposed method are introduced in Section 3.3. In Section 4, the simulation date is used to validate the proposed method, and the proposed method is compared with other methods. The experimental platform is described and the actual date of planetary gearbox is applied to validate the proposed method in Section 5. Finally, conclusions are summarized in Section 6.

II. A DESCRIPTION OF THEORETICAL BACKGROUND

A. VARIATIONAL MODE DECOMPOSITION THEORY

The VMD method can self-adaptively divide the signal frequency domain and effectively separate each component to obtain a series of modal components with sparse characteristics [17]–[19]. Therefore, the essence of VMD is to construct

and solve variational problems. Assuming that a signal is decomposed into K intrinsic mode functions by VMD algorithm, the construction process of the corresponding variational problem can be summarized as follows [20]:

Step 1: Hilbert transform is applied to each modal function $u_k(t)$ to obtain the signal-side spectrum of its analytic signal, as shown in Eq. (1):

$$\left(\delta(t) + \frac{j}{\pi t}\right) * u_k(t) \tag{1}$$

where $\delta(t)$ denotes the impulse function, j is the imaginary unit, $\{u_k(t)\} = \{u_1(t), u_2(t), \ldots, u_k(t)\}$ is the K decomposed modal functions, and $*$ represents convolution operation.

Step 2: The analytical signal of each modal function is mixed with the predicted estimated central frequency ω_k, and the spectrum of each modal function is modulated to the corresponding fundamental frequency band. The analytical signal of modal function is as follows:

$$\left[\left(\delta(t) + \frac{j}{\pi t}\right) * u_k(t)\right] e^{-j\omega_k t} \tag{2}$$

Step 3: The bandwidth of each modal function is estimated by calculating the squared L^2 -norm of the gradient of the analytic signal. The final constrained variational problem can be described by the following equation:

$$\begin{cases} \min\limits_{\{u_k\},\{\omega_k\}} \left\{ \sum\limits_{k=1}^{K} \left\| \partial_t \left[(\delta(t) + \frac{j}{\pi}) * u_k(t) \right] e^{-j\omega_k t} \right\|_2^2 \right\} \\ s.t \sum\limits_{k=1}^{K} u_k = f \end{cases} \tag{3}$$

where f is the original input signal, ∂_t denotes the partial derivative of a function, $\{\omega_k\} = \{\omega_1, \omega_2, \omega_3, \ldots, \omega_k\}$ is the central frequency of each modal function, and $\sum_k := \sum_{k=1}^{K}$ is the sum of all IMF components.

In order to solve the optimal solution of the constrained variational problem, the Lagrangian multiplier operator $\lambda(t)$ and penalty factor α are introduced. The extended Lagrange expression is presented as follows:

$$\begin{aligned} &L\left(\{u_k\}, \{\omega_k\}, \lambda\right) \\ &= \alpha \sum_k \left\| \partial_t \left[\left(\delta(t) + \frac{j}{\pi t}\right) u_k(t) \right] e^{-j\omega_k t} \right\|_2^2 \\ &\quad + \left\| f(t) - \sum_k u_k(t) \right\|^2 + \left\langle \lambda(t), f(t) - \sum_k u_k(t) \right\rangle \end{aligned} \tag{4}$$

The VMD algorithm uses the alternate direction method of multipliers (ADMM) to obtain the optimal solution of the extended Lagrange expression [21]–[23].

First, the number of modes K needs to be set artificially in advance. Meanwhile, the frequency domain expression of the modal function $\hat{u}_k^1$, the central frequency of each modal function ω_k^1 and the Lagrangian multiplier operator $\hat{\lambda}^1$ are initialized. Then, modal function u_k and their central frequency ω_k are updated respectively according to Eq.(5) and Eq.(6), respectively:

$$\hat{u}_k^{n+1} \leftarrow \frac{\hat{f} - \sum_{i<k} \hat{u}_i^{n+1} - \sum_{i>k} \hat{u}_i^n + \frac{\hat{\lambda}^n}{2}}{1 + 2\alpha(\omega - \omega_n^k)^2} \tag{5}$$

and

$$\omega_k^{n+1} \leftarrow \frac{\int_0^\infty \omega \left|\hat{u}_k(\omega)\right|^2 d\omega}{\int_0^\infty \left|\hat{u}_k(\omega)\right|^2 d\omega} \tag{6}$$

After each updating of the modal functions and the central frequencies, the Lagrangian multiplier operator is also updated by Eq.(7):

$$\hat{\lambda}^{n+1} \leftarrow \hat{\lambda}^n + \tau \left(\hat{f} - \sum_k \hat{u}^{n+1} \right) \tag{7}$$

The above update iteration continues until the convergence condition Eq.(8) is satisfied.

$$\sum_k \left\| \hat{u}_k^{n+1} - \hat{u}_k^n \right\|_2^2 / \left\| \hat{u}_k^n \right\|_2^2 < \varepsilon \tag{8}$$

where ε is the tolerance of the convergence criterion, and uses the default value of standard VMD.

B. SINGULAR VALUE DECOMPOSITION METHOD

Let $X = (x(1), x(2), \ldots, x(N))$ be a discrete signal with noise. Based on the theory of phase space reconstruction, the signal X can be constructed into Hankel matrix of order $m \times n$ [24]–[26]:

$$A = \begin{bmatrix} x(1) & x(2) & \cdots & x(n) \\ x(2) & x(3) & \cdots & x(n+1) \\ \vdots & \vdots & \vdots & \vdots \\ x(N-n+1) & x(N-n+2) & \cdots & x(N) \end{bmatrix} \tag{9}$$

where N is the length of the signal, $1 < n < N$, let $m = N - n + 1$, then $A \in R^{m \times n}$. The above real matrix A is also called the reconstruction of attractor orbit matrix [27].

The matrix A reflects the dynamic properties of the attractor in the reconstructed space by reconstructing the characteristics of the attractor. The SVD is performed on the above real matrix A, the following relational equation can be obtained:

$$A = USV^T \tag{10}$$

where $U = [u_1, u_2, \ldots, u_m] \in R^{m \times n}$ and $V = [v_1, v_2, \ldots, v_n] \in R^{m \times n}$ are orthogonal matrices, $S = [diag(\delta_1, \delta_2, \ldots, \delta_q), 0] \in R^{m \times n}$ or its transposition depends on $m \leq n$ or $m > n$, 0 represents a zero matrix, where $q = \min(m, n)$, and $\delta_1 \geq \delta_2 \geq \ldots \geq \delta_q \geq 0$ are the singular values of matrix A.

According to Eq. (10), the Hankel matrix A can be represented by column vectors u_i and v_i, i.e.:

$$A = \delta_1 u_1 v_1^\tau + \delta_2 u_2 v_2^\tau + \ldots + \delta_q u_q v_q^\tau \tag{11}$$

where $u_i \in R^{m \times 1}$, $v_i \in R^{n \times 1}$, $i = 1, 2 \ldots, q$, $q = \min(m, n)$, let $A_i = \delta_i u_i v_i^\tau$, then $A_i \in R^{m \times n}$. Let A_i denote the first row

vector of $P_{i,1}$, and $H_{i,n}$ denotes the sub-column vector of A_i after removing the first element from the last column vector. According to the construction process of Hankel matrix, it can be seen that a component signal P_i can be formed by connecting the beginning and end of the transposition of $P_{i,1}$ and A_i. P_i can be represented in the form of a vector as follows:

$$P_i = \left(P_{i,1}, H_{j,n}^T\right); H_{i,1} \in R^{(m-1)\times 1}, P_{i,1} \in R^{1\times n}. \quad (12)$$

The linear superposition of all component signals P_i forms a decomposition of the original signal X, i.e.:

$$X = P_1 + P_2 + P_3 + ... + P_n \quad (13)$$

The order of component signals is arranged from high to low according to the corresponding size of singular values δ_i [28], [29].

C. COSINE SIMILARITY INDEX

Cosine similarity is a method to measure the similarity between two objects [33]. First, the two signals are mapped to the vector space, and then the cosine value of the angle between two vectors is measured in the inner product space to measure the similarity between them [34]. The more common components between the two signals, the closer their cosine similarity value is to 1. On the contrary, the closer the cosine similarity is to 0. The two vibration signals are defined as $X_1(n)$ and $X_2(n)$, and the calculation formula of the cosine similarity of the two signals is as shown in Eq. (14):

$$C_S(X_1, X_2) = \left| \frac{\sum_{n=1}^{N} X_1(n)X_2(n)}{\sqrt{\sum_{n=1}^{N} X_1^2(n)}\sqrt{\sum_{n=1}^{N} X_2^2(n)}} \right| \quad (14)$$

In the actual operation of planetary gearbox, the vibration signal contains not only weak fault impulse components, but also heavy background noise and other interference components. Therefore, the cosine similarity index can be used to select useful component signals. The component signal that the largest cosine similarity with the original signal is considered to be the real fault signal, and is selected as the sensitive component. The remainder components are considered as noise or interference component will be eliminated, thereby improving the signal-to-noise ratio of the signal.

III. THE PROPOSED METHODS

A. ADAPTIVE PARAMETER OPTIMIZED VMD

According to the description in section 2.1, the decomposed mode number K and penalty factors α need to be preset by users in the VMD algorithm, which will significantly influence the adaptability of the VMD. The original signal is decomposed by VMD to obtain K modal components, and each modal component $u_k(t)$ corresponds to a central frequency $\omega_k(t)$. The parameters K and α have a close relationship with $\omega_k(t)$, and will directly determine the decomposition performance of the VMD algorithm. At present, the number of modal K is determined by the observation center frequency method in most cases, and the value of penalty factor α is the default value in the VMD algorithm. However, this method requires users to continuously modify the parameters K and α in order to avoid the central frequencies of two adjacent modes overlapping, which also lacks self-adaptability. In order to adaptively determine the optimal parameters, an adaptive parameter optimized VMD (APOVMD) method is proposed. The principle of this new method is to determine the optimal parameter combination according to compare the ratio of the central frequency of two adjacent modes with the threshold value under the same K and α. In this paper, according to the frequency band characteristics of the early fault signal of the planetary gearbox, and through multiple experiments, the threshold value θ is set to 1.2. The flow chart of APOVMD algorithm is shown in Fig. 1, and the specific implementation steps are as follows:

Step 1: Input the original signal $x(t)$.

Step 2: Initialize modal umber $K = 2$ and penalty factor $\alpha = 100$. (In this paper, the maximum number of iterations $\alpha = 3000$ and the size of search step is 100.)

Step 3: Decompose the signal by using the VMD algorithm to obtain K modal components and their corresponding central frequencies $\omega_k(t)$.

Step 4: Divide the center frequency of the latter model component u_k by the center frequency of the former component u_{k-1} to obtain a set of frequency ratios $\lambda_1, \lambda_2, \cdots, \lambda_{K-1}(\lambda_k = \omega_{K-1}/\omega_K, k = 1, 2...K-1)$.

Step 5: Set the threshold $\theta = 1.2$. When $\lambda_k > \theta$, it is considered that the VMD decomposition is not enough. Therefore, let $K = k+1, \alpha = \alpha+100$, and return step 3 to 4.

Step 6: When $\lambda_k \leq \theta$, it is considered that the center frequencies of u_k and u_{k-1} are similar, and the VMD has been over decomposed. Therefore, the optimal parameters $K = K-1, \alpha = \alpha-100$ are obtained, and the best decomposition result is output.

B. CONCEPT OF SINGULAR KURTOSIS DIFFERENCE SPECTRUM

Reference [29] proposed the method of singular value difference spectrum for selecting the effective reconstruction order of SVD. This method is now usually used to select the order of reconstructed signal in the field of mechanical fault diagnosis. However, when the fault information is weak, if only the order corresponding to the maximum peak point in the singular value difference spectrum is selected for signal reconstruction, some weak impact signal characteristics will be lost, and the true fault signal cannot be restored.

Kurtosis is very sensitive to the impact characteristics of the signal [35], [36]. When the gear occur a local fault, the impact characteristic will appear in the vibration signal. Therefore, kurtosis can be used as a basis for selecting effective singular values. It can be expressed as:

$$k = \frac{E(x(t)-\mu)^4}{\sigma^4} \quad (15)$$

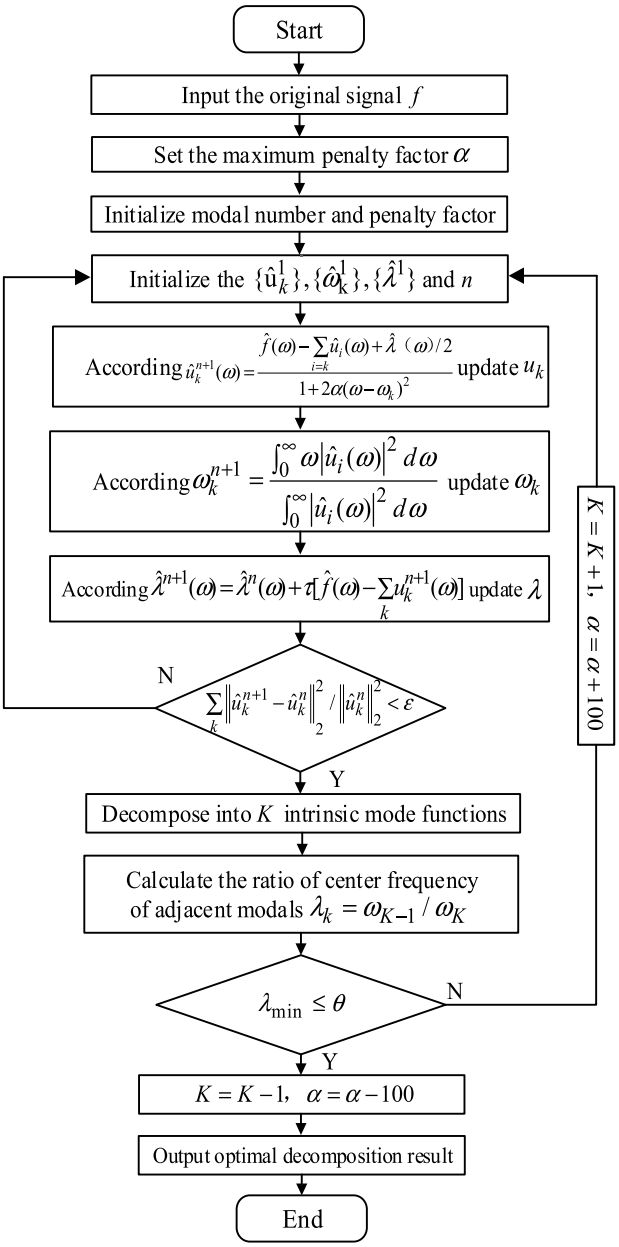

FIGURE 1. The flow chart of APOVMD algorithm.

where k denotes kurtosis, $x(t)$ is the fault vibration signal, μ is the mean of $x(t)$, σ is the standard deviation of $x(t)$.

In order to accurately retain useful fault characteristics and minimize the effects of noise, the method of singular kurtosis difference spectrum is introduced in this paper based on the traditional singular value decomposition. It can be calculated as follows:

$$SKD_i = dk(i+1) - dk(i)(i = 1, 2, \ldots, q-1) \quad (16)$$

In the Eq.(16), SKD_i is the kurtosis value of the first i-order reconstructed signal, i is the number of singular values defined in Section 2.2. When the kurtosis values of two adjacent reconstructed signals differ greatly, a significant peak will be generated in the differential spectrum, and there will inevitably be a maximum peak in the entire differential spectrum, which is the maximum mutation position l of the kurtosis value. The maximum mutation point not only reflects that the reconstructed signal contains abundant fault impact characteristics, but also shows that the nature of signal has changed fundamentally, which is also a natural reflection of the transformation between useful signal and noise signal. Therefore, the optimal separation of useful signals from noise can be achieved by selecting the singular values of the first l-order for signal reconstruction.

C. THE IMPLEMENTATION PROCESS OF THE PROPOSED METHOD

The early fault signal of planetary gearbox has the characteristics of weak feature information, easy to be submerged by noise and low signal-to-noise ratio. The weak periodic impact characteristics caused by the fault are often submerged by strong background noise, which can not be effectively extracted. Therefore, the key to early fault diagnosis of planetary gearbox is to effectively extract the weak fault features implied in the vibration signals. In this paper, the APOVMD algorithm is used to decompose the early fault signal of planetary gearbox, which can avoid the disadvantage of relying on human experience to select decomposed parameters in VMD. The signal-to-noise ratio of planetary gearbox fault signal can be significantly improved by using APOVMD algorithm. The fault characteristics of the original vibration signal submerged by noise can be effectively highlighted, but there will still be more noise interference. Although the SVD can effectively eliminate the noise interference in the signal, the reconstructed order can not be accurately determined. Therefore, a singular kurtosis difference spectrum method is proposed, which can adaptively select the effective reconstructed order, and finally eliminate the influence of residual noise. Based on the above analysis, a weak fault feature extraction method of planetary gearbox based on APOVMD and singular kurtosis difference spectrum is proposed in this paper, which is expected to achieve accurate identification of early fault of planetary gearbox.

The diagnostic process is shown in Fig. 2. The specific implementation process is as follows:

Step 1: Collect the planetary gearbox fault vibration signal.

Step 2: The original vibration signal of planetary gearbox is decomposed by APOVMD method, and a series of modal components are obtained.

Step 3: The cosine similarity index is used to select the model component that contains the most abundant fault feature information as the sensitive component.

Step 4: The SVD is performed on the sensitive component, and the reconstructed order is adaptively determined by singular kurtosis difference spectrum method for signal noise reduction.

Step 5: Hilbert envelope demodulation analysis is applied to reconstructed signal to extract fault characteristic frequency information of planetary gearbox, and compare it with

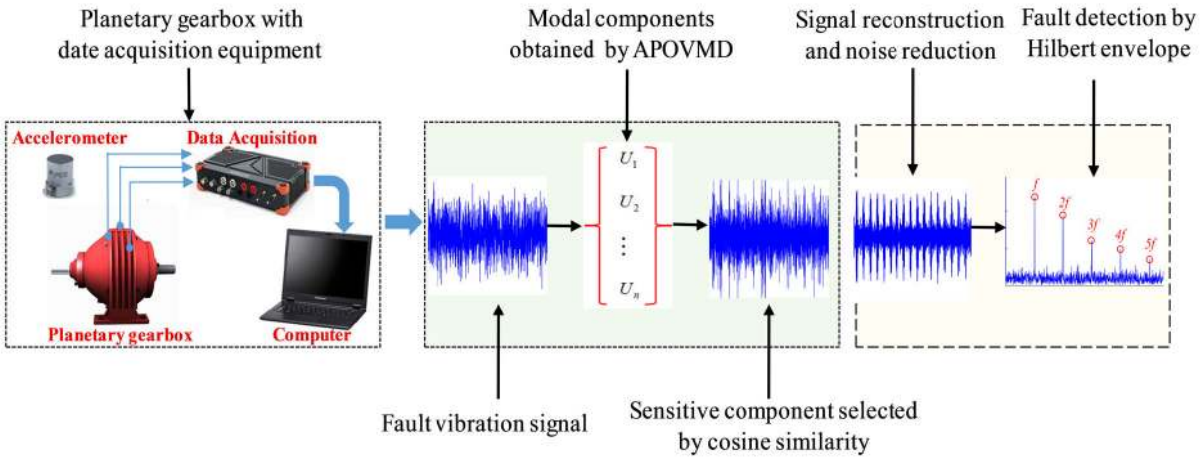

FIGURE 2. The flowchart of the proposed method.

the theoretical value to determine the fault location of the gear.

IV. STUDY ON SIMULATED SIGNAL

When a local fault occurs in the gear of the planetary gearbox, the fault vibration signal collected by the acceleration sensor can be represented by an AM-FM signal model. The carrier frequency is the gear meshing frequency or its frequency multiplication, and the modulation frequency is the fault gear characteristic frequency or its

frequency multiplication. In order to facilitate the analysis, only the fundamental frequency of the modulation frequency and the carrier frequency are considered when establishing the planetary gearbox AM-FM vibration signal model, that is, the frequency component only includes the gear meshing frequency and the fault gear characteristic frequency. Therefore, the simplified model of the sun gear fault vibration signal is constructed as follows [37], [38]:

$$x(t) = \underbrace{[1-\cos(2\pi f_{sr}t)][1+\cos A(2\pi f_s t)]}_{\text{AM by gear fault}} \times \cos[2\pi f_m t + \underbrace{B\sin(2\pi f_s t)}_{\text{FM by gear fault}} + \phi] + \underbrace{n(t)}_{\text{Noise}} \quad (17)$$

where the sun gear absolute rotation frequency $f_{sr} = 25$ Hz, the sun gear fault characteristic frequency $f_s = 70$ Hz, the gear meshing frequency $f_m = 1000$ Hz, $A = B = 1$ is the modulation coefficient of AM and FM respectively, and ϕ is the initial phase. In order to verify the ability of the proposed method to extract the early weak features of the sun gear under heavy background noise, the white Gaussian noise $n(t)$ with SNR of -18dB is added to the simulated shock signal shown in Eq. (17) by using the MATLAB function AWGN(x, SNR). Meanwhile, the sampling frequency of the simulation signal is set to 10240Hz and the sampling time length is 1s.

The time domain waveform and its frequency spectrum of the simulated signal under heavy background noise are shown in Fig. 3. It can be seen from Fig. 3(b) and(c) that the heavy background noise has completely submerged the original periodic impact features of the time domain signal, and there is no sign of the sun gear fault characteristics in the simulated signal.

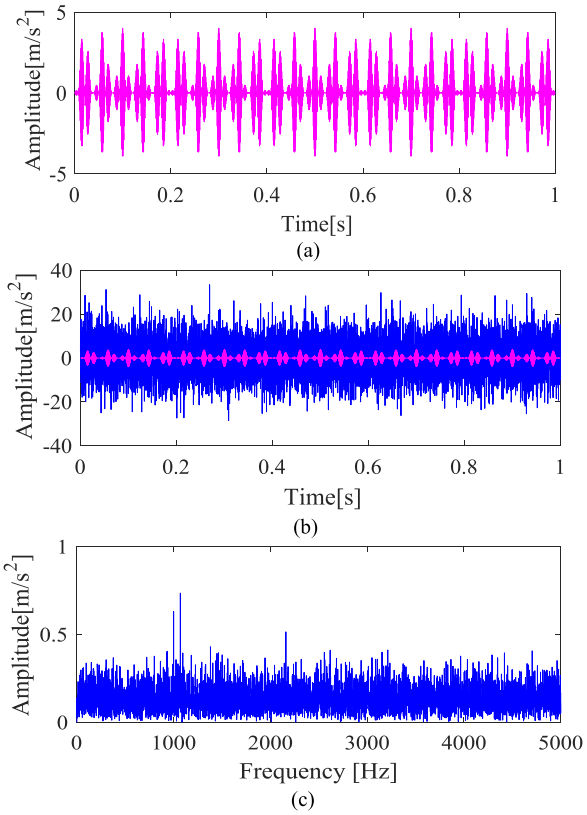

FIGURE 3. The time domain and frequency domain analysis of simulated signal: (a) the time domain waveform of simulated fault signal, (b) the time domain waveform of noise-added mixture signal, (c) the frequency spectrum of simulated signal.

First, the signal in Fig. 3(b) is decomposed by the APOVMD method. In order to illustrate the influence of

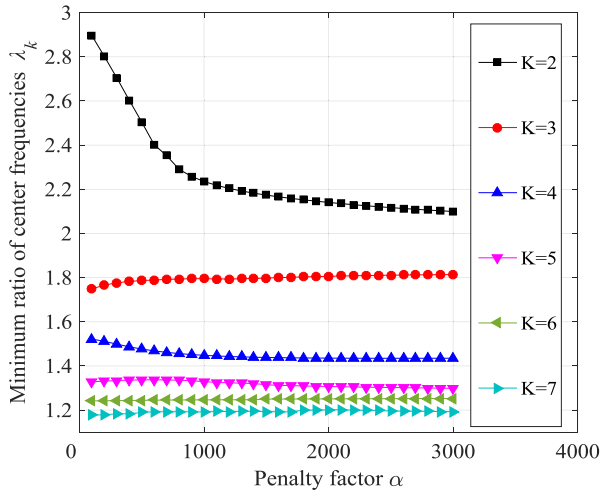

FIGURE 4. The ratio of center frequencies of adjacent modes.

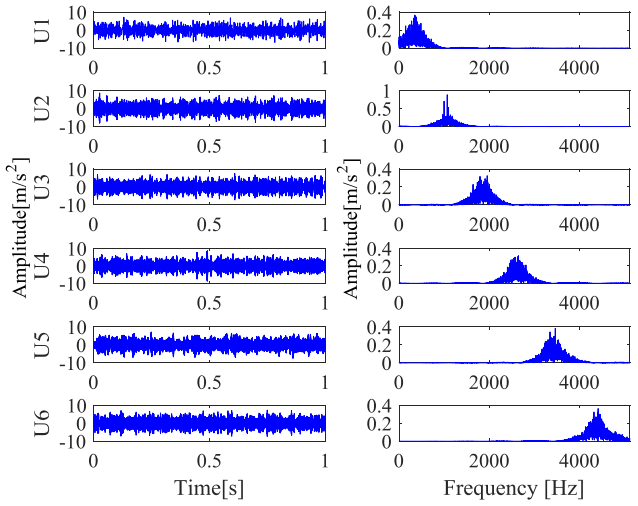

FIGURE 5. Modal components and their spectrum of simulated signal decomposed by APOVMD.

mode number K and penalty factor α on modal center frequency and the universality of the proposed method, the experiment in Fig. 4 is repeated 50 times, and the average statistical results is reported. After summing and averaging, the ratio of center frequencies of adjacent modes under different decomposed mode number K sand penalty factors α are shown in Fig. 4. It can be found from Fig. 4 that when $K \geq 7$, the ratio of center frequency begins to be less than the threshold value $\theta = 1.2$, and VMD is considered to be over decomposed. Meanwhile, when α is between 1000 and 3000, the ratio of center frequency changes slightly and tends to be flat. Therefore, the signal in Fig. 3 (b) is decomposed by APOVMD, which the mode number and penalty factor are set to $K = 6$ and $\alpha = 1500$, respectively. Fig. 5 shows the decomposed modal components and their frequency spectrum. The cosine similarity index is used to determine the sensitive component from the decomposed modal components.

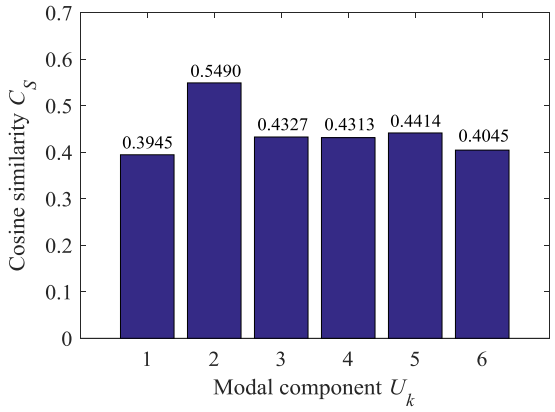

FIGURE 6. The cosine similarity between the decomposed modal signals and the original signal.

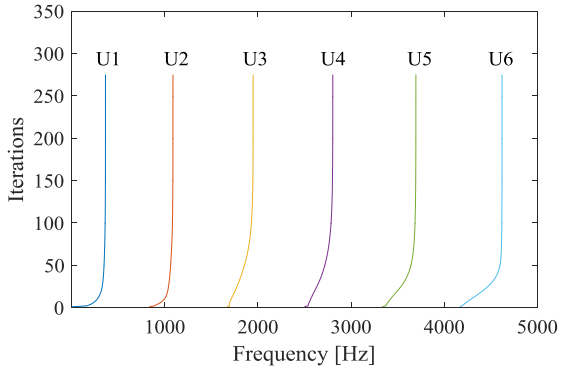

FIGURE 7. The number of iterations of modal center frequencies.

The cosine similarity between modal components and the original signal is shown in Fig. 6. As can be seen from Fig. 6, the cosine similarity of U2 is the largest, so U2 is selected as the sensitive component for the next analysis. Fig. 7 shows the number of the central frequencies iterations of the modal components obtained by the APOVMD method. It can be found that the central frequency of U2 component is 1073Hz, which is very close to the gear meshing frequency 1000Hz. Gear fault information is mainly carried by the gear meshing frequency or its frequency multiplication component. Therefore, the U2 sensitive component selected by cosine similarity index contains abundant gear fault information.

Then, the Hankel matrix with 500 rows is constructed for the U2 component and decomposed by SVD. The singular kurtosis difference spectrum method is employed to determine the effective reconstructed order for noise reduction. In order to clearly observe the variation of singular kurtosis difference spectrum, only the first 50 data points are plotted in the same coordinate system, as shown in Fig. 8. As provided in Fig. 8, the position of the maximum mutation point occurs at the order of singular value is 14, thus the first fourteen singular values are selected for signal reconstruction, and the reconstructed result is shown in Fig. 9(a). It is found that the reconstructed signal actually restores the original sun gear fault simulation signal.

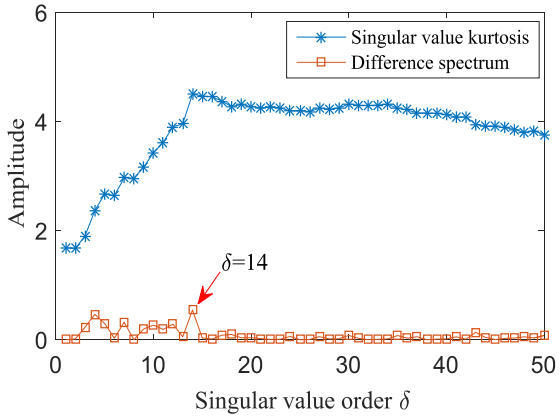

FIGURE 8. Singular kurtosis difference spectrum of the U2 sensitive component.

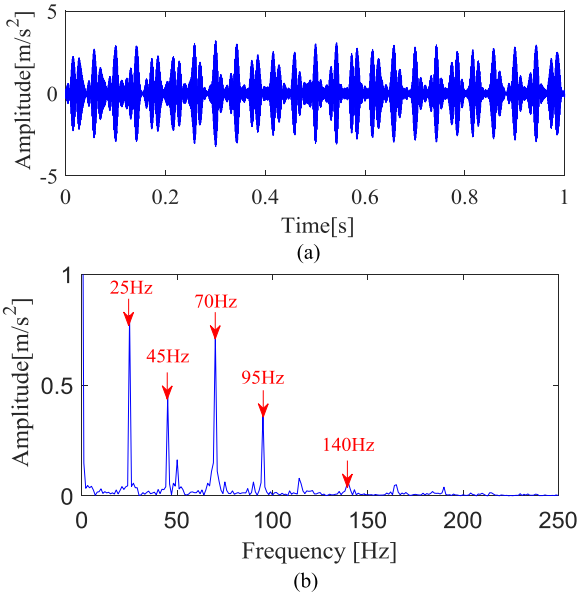

FIGURE 9. The result of simulated signal by the proposed method: (a) the reconstructed signal obtained by the proposed method, (b) the envelope spectrum of the reconstructed signal.

Fig. 9(b) shows the envelope spectrum of the reconstructed signal, it can be clearly seen that the sun gear fault characteristic frequency 70Hz and its twice 140Hz, the sun gear absolute rotation frequency 25Hz, and the sun gear fault characteristic frequency plus or minus the sun gear absolute rotation frequency 70Hz ± 25Hz are prominent. The above analysis results accord with the sun gear fault characteristics in envelope spectrum.

For comparison, the direct envelope demodulation analysis of the U2 component obtained by the APOVMD method is performed, and the result is provided in Fig. 10. In the envelope spectrum of U2 component, we can note that although there are peaks at the sun gear fault characteristic frequency, the peaks at other interference frequencies are also plentiful,

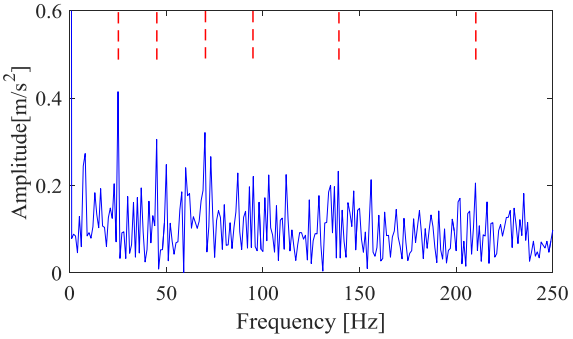

FIGURE 10. Direct envelope analysis of U2 modal component.

which cause serious interference to the identification of the sun gear fault characteristic information.

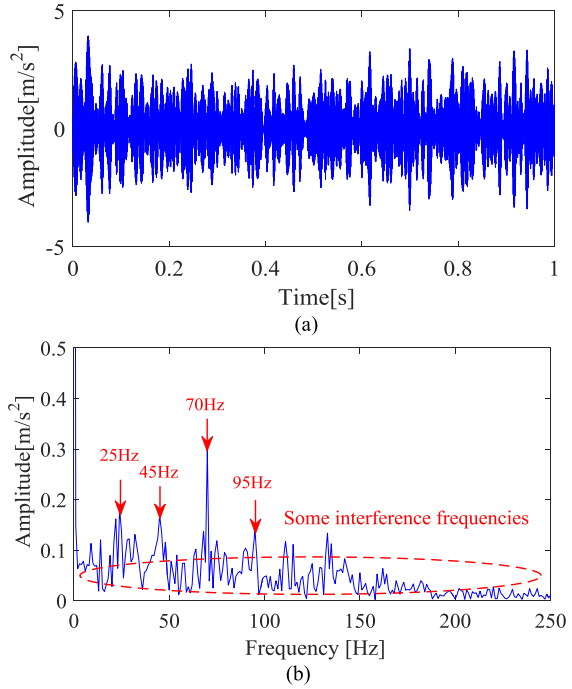

FIGURE 11. Comparative analysis of simulated signal processed by VMD-SVD method: (a) the reconstructed signal obtained by VMD-SVD method, (b) the envelope spectrum of the reconstructed signal.

Fig. 11 presents the processing result of the original fault simulation signal by the VMD-SVD method. In the reconstructed signal shown in Fig. 11(a), the original fault signal can not be accurately restored. In the envelope spectrum shown in Fig. 11(b), although the sun gear fault characteristic frequency information can be found, the extracted result is not as ideal as in the Fig. 9(b).

Fig. 12 shows the processing result of the original fault simulation signal by the EEMD-SVD method. From the reconstructed signal of Fig. 12(a), it can be seen that the reconstructed signal is distorted and the original fault signal can not be restored. From the envelope spectrum of Fig. 12(b), it can be observed that there is a peak at the sun gear fault

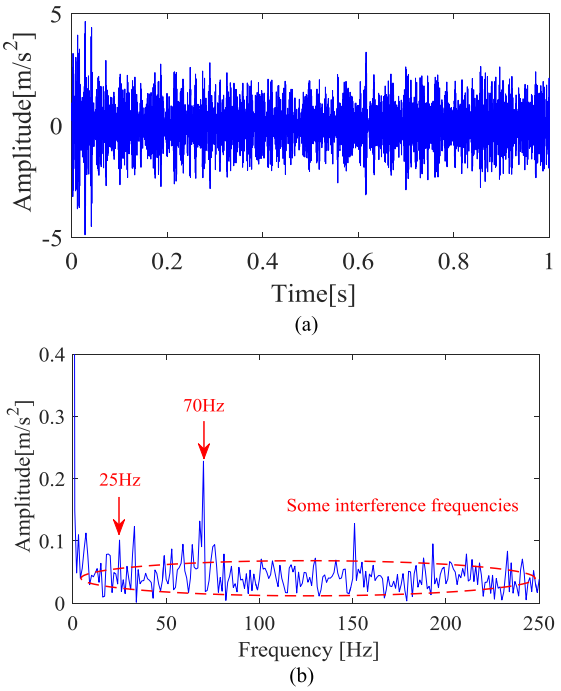

FIGURE 12. Comparative analysis of simulated signal processed by EEMD-SVD method: (a) the reconstructed signal obtained by EEMD-SVD method, (b) the envelope spectrum of the reconstructed signal.

characteristic frequency of 70Hz, but other fault frequency information is not obvious. The result indicates that the EEMD-SVD method can not effectively extract fault feature information.

Through the above comparison and analysis, we can conclude that under the strong background noise interference, the VMD-SVD method and EEMD-SVD method are difficult to extract the fault feature information of the sun gear. Only the method proposed in this paper can accurately and comprehensively extract the weak sun gear fault feature hidden in the dynamic signal. Therefore, the effectiveness and superiority of the proposed method in extracting the early weak fault feature of planetary gearbox are also verified.

V. EXPERIMENTAL VERIFICATION

A. EXPERIMENTAL EQUIPMENT

In order to verify the effectiveness of the proposed method in the actual planetary gearbox fault diagnosis, the Spectra Quest synthetic experimental platform for the planetary gearbox fault is used in this study. The experimental system and its three-dimensional model are shown in Fig. 13. The test bench is mainly composed of a variable speed drive motor, a torsion sensor and encoder, a two-stage planetary gearbox, a parallel shaft gearbox and a programmable magnetic brake. There are three planetary gears in the first stage planetary gearbox and four planetary gears in the second stage planetary gearbox. The first stage sun gear is connected with the drive shaft of the motor, and the second stage planetary carrier is connected with the input shaft of the parallel axis gearbox. During the

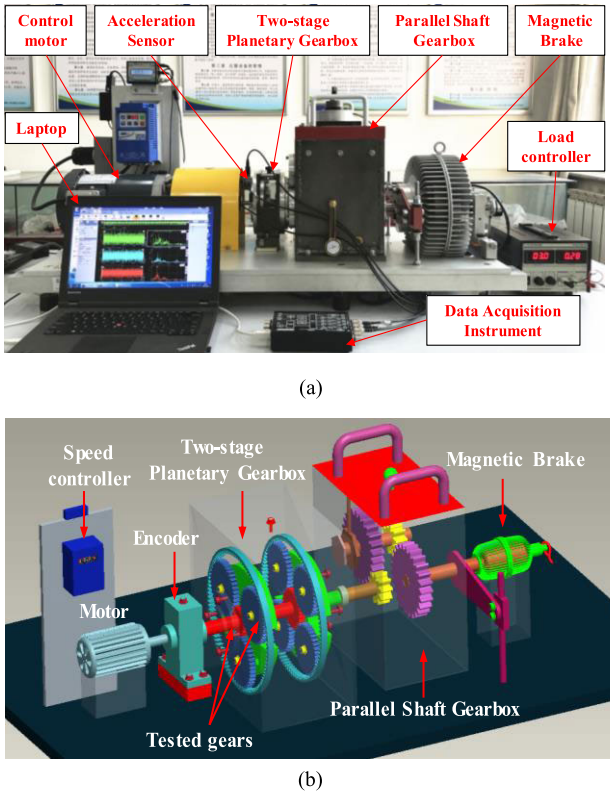

FIGURE 13. The test bench of planetary gearbox fault diagnosis and its three-dimensional: (a) experimental platform for the planetary gearbox faults, (b) three-dimensional model of experimental platform.

TABLE 1. Basic parameters of two-stage planetary gearbox.

Gear type	Number of gear teeth	
	Input stage	Output stage
Ring	100	100
Planet	40(3 planets)	36(4 planets)
Sun	20	28

experiment, the faulty gears are installed in the first planetary gearbox for testing. The parameters of planetary gearbox are shown in Table 1. In order to simulate a local fault of the gear, the micro-crack with a width of 0.15mm and a depth of 1mm is machined along the root direction on the gear teeth of the sun gear and the planetary gear by wire cutting technology. The faulty gears are shown in Fig. 14. The fault vibration signal is collected by using PCB 352C33 accelerometer (acceleration range of $\pm$ 50g, frequency range of 0.5–10kHz, and sensitivity is 100 mV/g). The accelerometers are mounted on the vertical, horizontal and axial test points of the planetary gearbox housing to measure vibration signals. DT9837 data conversion instrument and a computer with DAQ software are selected as the data acquisition system in this experiment. The speed of the sun gear connected with the driving motor is 1380r/min during the experiment. The sampling frequency is 5120Hz, and the sampling time length is 5s. According to the structure parameters of planetary gearbox and the

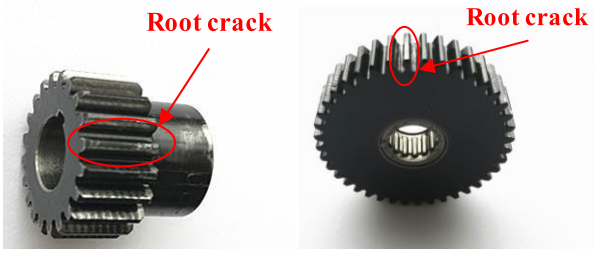

FIGURE 14. Gear fault states: (a)sun gear, (b) planetary gear.

speed of input shaft of sun gear, the local fault characteristic frequencies of each gear are calculated as shown in Table 2.

TABLE 2. Fault feature frequencies of the first stage planetary gear.

Meshing frequency	Absolute rotation frequency		Local fault characteristic frequency		
	Sun	Planetary	Sun	Planetary	Ring
383.33	23	3.83	19.17	9.58	11.50

B. CASE I: FAULT DETECTION OF SUN GEAR

Fig. 15 shows the time domain waveform and its frequency spectrum of the sun gear fault vibration signal measured by the acceleration sensor in the vertical direction. From the time domain waveform of Fig. 15(a), it is difficult to observe the regular impulse signal caused by the fault due to the noise interference. From the frequency spectrum of Fig.15 (b), the frequency component is very complex and no obvious characteristic frequency components can be found.

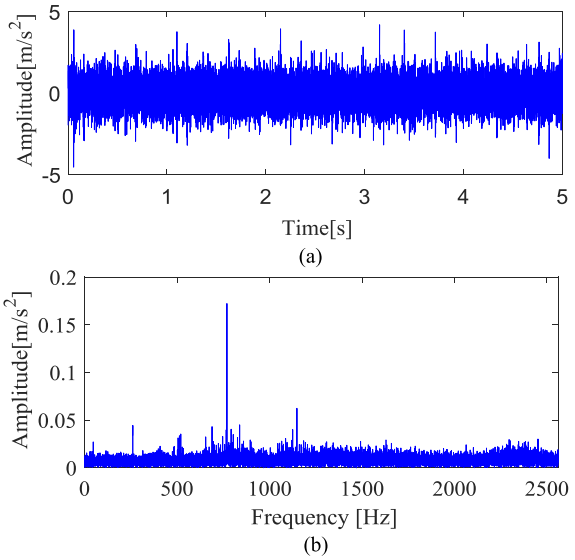

FIGURE 15. The time domain and frequency domain analysis of sun gear fault signal: (a) the time domain waveform of sun gear fault signal, (b) the frequency spectrum of sun gear fault signal.

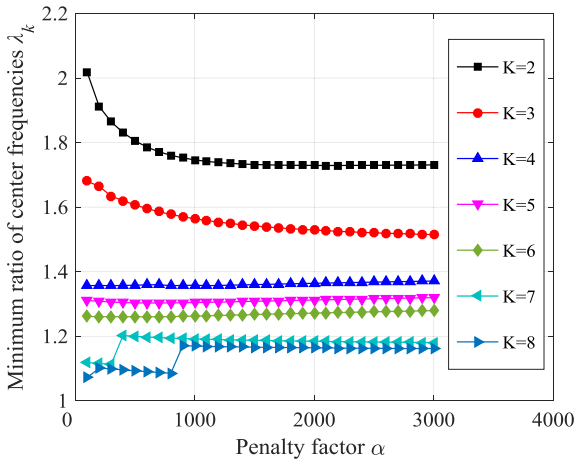

FIGURE 16. The ratio of center frequencies of adjacent modes.

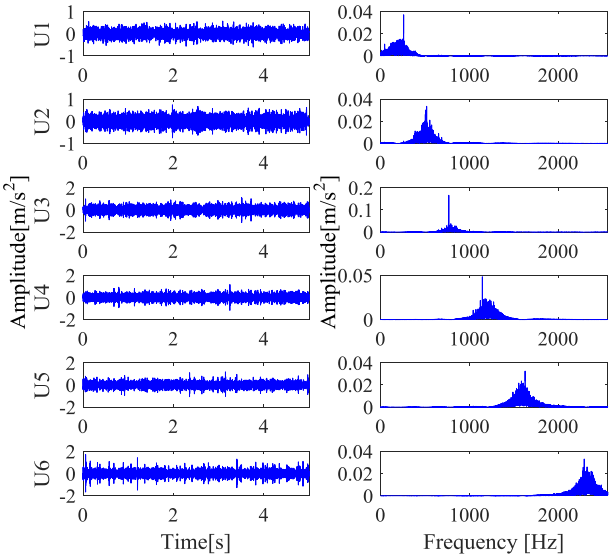

FIGURE 17. Modal components and their spectrum of sun gear fault signal decomposed by APOVMD.

In order to effectively extract the sun gear early fault characteristics, the proposed method is applied to process the sun gear fault vibration signal. First, the sun gear fault vibration signal is decomposed by the APOVMD method. Fig. 16 presents the radio of center frequencies of adjacent modes under different mode numbers K and penalty factor α. As displayed in Fig. 16, when the value of K is more than 6, the ratio of center frequencies begin to be less than the threshold value $\theta = 1.2$, and VMD is considered to be over decomposed. Meanwhile, when α is between 1000 and 3000, the ratio of the entire center frequency changes slightly and tends to be stable. Therefore, the sun gear fault vibration signal is decomposed by APOVMD under the mode number $K = 6$ and the penalty factor $\alpha = 2000$. Fig. 17 illustrates the decomposed modal components and their frequency spectrum. The cosine similarity index is used to select sensitive component from the decomposed modal components.

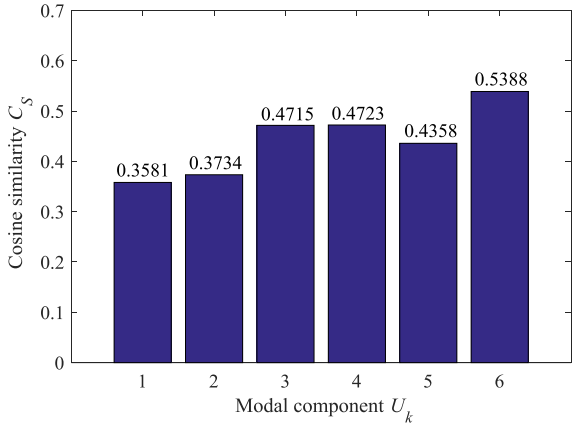

FIGURE 18. The cosine similarity between the decomposed modal signals and the original signal.

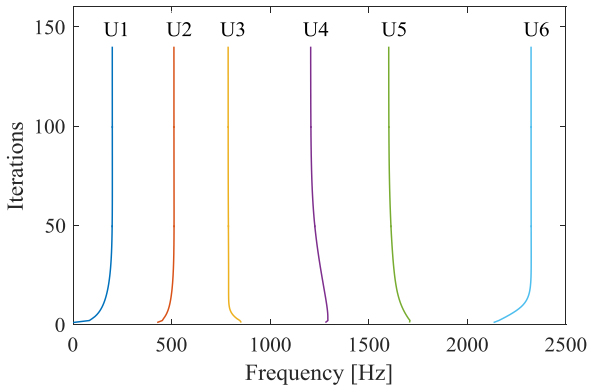

FIGURE 19. The number of iterations of modal center frequencies.

The cosine similarity between modal components and the original signal is given in Fig. 18, one can also find that the cosine similarity value of U6 is the largest. Therefore, the U6 is selected as the sensitive component for the next analysis. Fig. 19 shows the number of the central frequencies iterations of the modal components obtained by the APOVMD method. It can be seen that the central frequency of U6 component is 2324Hz, which is very close to the six times gear meshing frequency 2299.8Hz. Gear fault information is mainly carried by the gear meshing frequency or its frequency multiplication. Therefore, the U6 sensitive component selected by cosine similarity index contains the abundant gear fault information.

Then, the Hankel matrix with 500 rows is constructed for the U6 sensitive component and decomposed by SVD. The singular kurtosis difference spectrum method is employed to determine the effective reconstructed order for signal noise reduction. In order to clearly observe the variation of singular kurtosis difference spectrum, only the first 50 points are plotted here, as shown in Fig. 20. As can be seen from Fig. 20, the maximum mutation point occurs at the location where the order of singular value is 11. Therefore, the first eleven singular values are reconstructed to obtained de-noised signal.

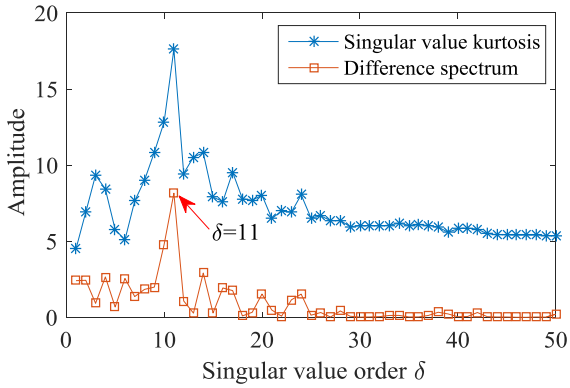

FIGURE 20. Singular kurtosis difference spectrum of the U6 sensitive component.

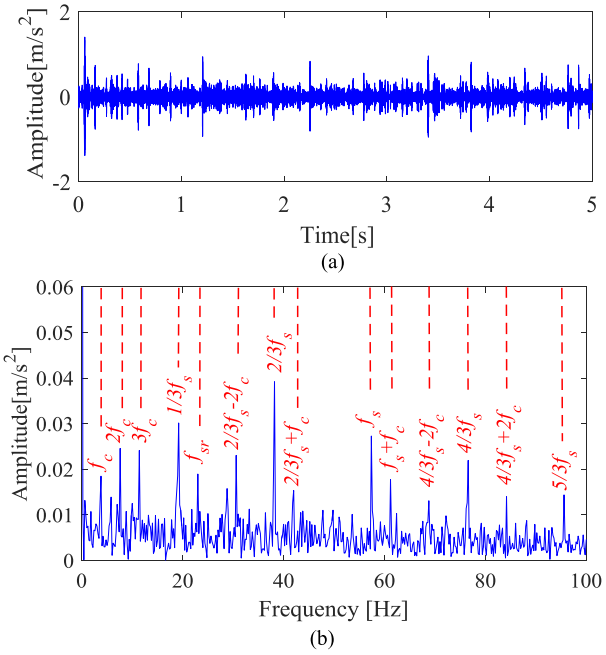

FIGURE 21. The processing result of sun gear fault signal by the proposed method: (a) The reconstructed signal obtained by the proposed method, (b) The envelope spectrum of the reconstructed signal.

Fig. 21(a) illustrates the reconstructed signal, from which regular impulse components caused by faults can be clearly observed.

Fig. 21(b) shows the envelope spectrum of the reconstructed signal, it can be seen that one third of the sun gear fault characteristic frequencies $1/3f_s$ and its harmonics $n/3f_s$ are dominant. (For the actual planetary gearbox, the planetary gears may not be identical because of processing or manufacturing errors. The fault impact generated when the three planetary gears mesh with the sun gear fault teeth is considered as three different impact sequences. As a result, one third of the sun gear fault characteristic frequencies and its harmonics appear in the envelope spectrum.) Moreover, other peaks in the envelope spectrum exist at the sun gear absolute rotation frequency f_{sr}, the planet carrier rotating

frequency f_c and its harmonics mf_c, and the combination frequency $n/3f_s \pm mf_c(m, n = 1, 2, \cdots)$. These features indicate that a local fault has occurred in the sun gear, which is consistent with the actual experimental setting.

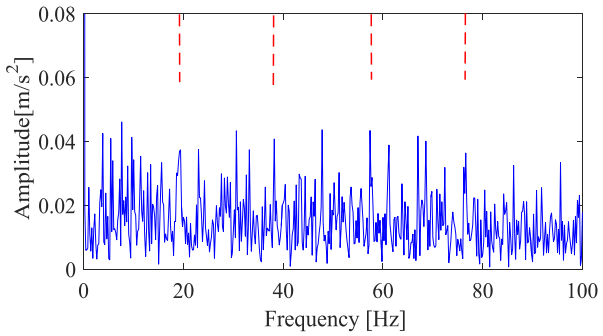

FIGURE 22. Direct envelope analysis of U6 modal component.

For comparison, the direct envelope demodulation analysis of the U6 sensitive component obtained by APOVMD decomposition is performed, and the envelope spectrum is given in Fig. 22. It can be found that although some peaks appear at the sun gear fault characteristic frequency, the peaks at other interference frequencies are also abundant, which cause serious interference to the identification of the fault characteristic information in the envelope spectrum. Therefore, it is difficult to provide strong evidence for the reasonable fault diagnosis of sun gear.

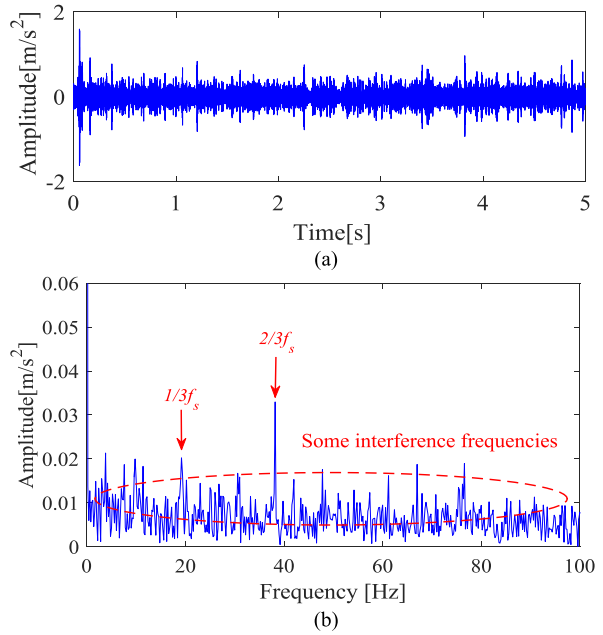

FIGURE 23. Comparative analysis of sun gear fault signal processed by VMD-SVD method: (a) The reconstructed signal obtained by VMD-SVD method, (b) The envelope spectrum of the reconstructed signal.

The VMD-SVD method is applied to analyze the same sun gear fault signal shown in Fig. 23. The reconstructed signal is displayed in Fig. 23(a), it can be seen that although some impact components appear in the reconstructed signal, the regularity and characteristics of these impacts are not obvious. The envelope spectrum of the reconstructed signal is shown in Fig. 23(b), from which we can only observed one third of the sun gear fault characteristic frequency $1/3f_s$ and its second harmonic $2/3f_s$, while other interference frequencies unrelated to the fault are also very rich, and the analysis results is not good as shown in Fig. 21(b).

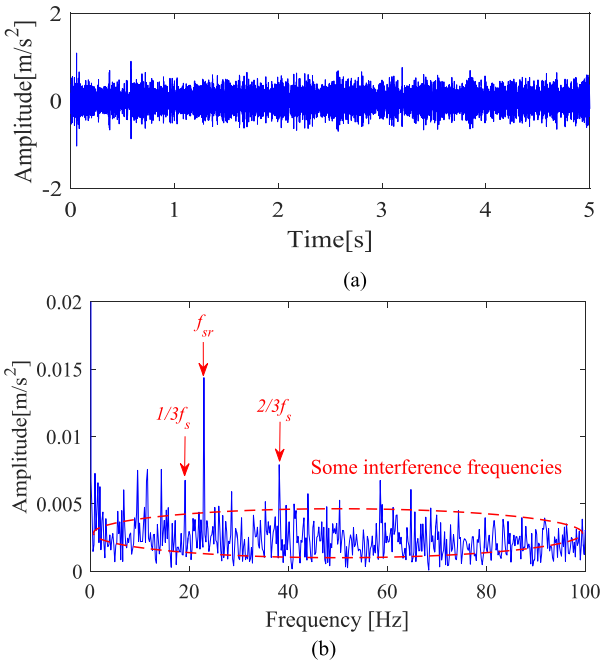

FIGURE 24. Comparative analysis of sun gear fault signal processed by EEMD-SVD method: (a) The reconstructed signal obtained by EEMD-SVD method, (b) The envelope spectrum of the reconstructed signal.

The EEMD-SVD method is used to analyze the same sun gear fault signal shown in Fig. 24. The reconstructed signal is provided in Fig. 24(a), it can be observed that there is no obvious periodic fault impact feature in the reconstructed signal. Fig. 24(b) presents the envelope spectrum of the reconstructed signal, it can be seen that only the sun gear absolute rotation frequency is prominent, and the sun gear fault frequency characteristic and its harmonic are not obvious, which makes the analysis result unsatisfactory.

C. CASE II: FAULT DETECTION OF PLANETARY GEAR

The time domain waveform and its spectrum of the planetary gear fault vibration signal measured by the acceleration sensor in the vertical direction are as shown in Fig. 25. It can be found that the time domain signal has no obvious periodic impact characteristics caused by the planetary gear fault. Moreover, it is difficult to identify the planetary gear crack fault symptoms in its frequency spectrum.

In order to extract the planetary gear fault symptoms, the proposed method is applied to process the planetary gear fault vibration signal. First, the planetary gear fault vibration signal is decomposed by the APOVMD method, in which the

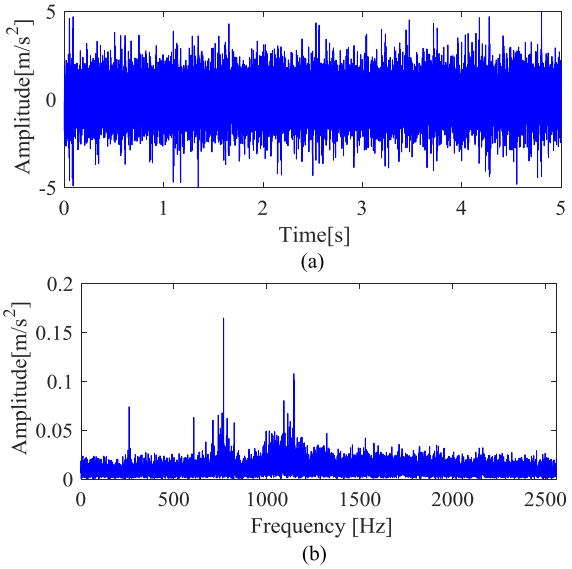

FIGURE 25. The time domain and frequency domain analysis of planetary gear fault signal: (a) The time domain waveform of planetary gear fault signal; (b) The frequency spectrum of planetary gear fault signal.

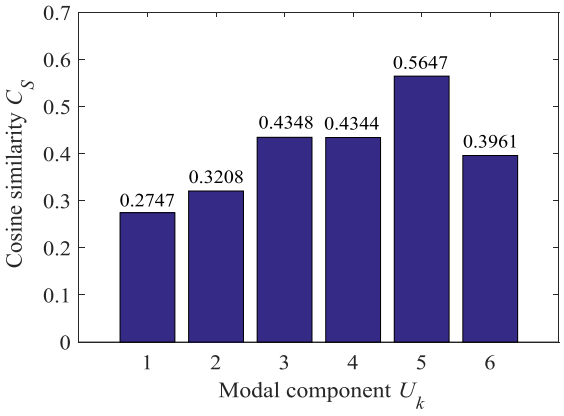

FIGURE 26. The cosine similarity between the decomposed modal signals and the original signal.

decomposed mode number and the penalty parameter are set to $K = 6$ and $\alpha = 2300$, respectively. Fig. 26 presents the cosine similarity between decomposed modal components and original signal, from which the cosine similarity value of U5 is the largest. Therefore, the U5 is selected as the sensitive component. Fig. 27 shows the number of the central frequencies iterations of the modal components obtained by the APOVMD method. It can be noted that the central frequency of U5 sensitive component is 1534Hz, which approximates the four times of the gear meshing frequency 1533.2Hz. Therefore, it also indicates that the U5 sensitive component contains a wealth of the gear fault information, which is suitable for the further research object. Then, the Hankel matrix with 500 rows is constructed for U5 component and decomposed by SVD. There constructed signal order is determined according to the singular kurtosis difference spectrum method. Only the first 50 points of the singular

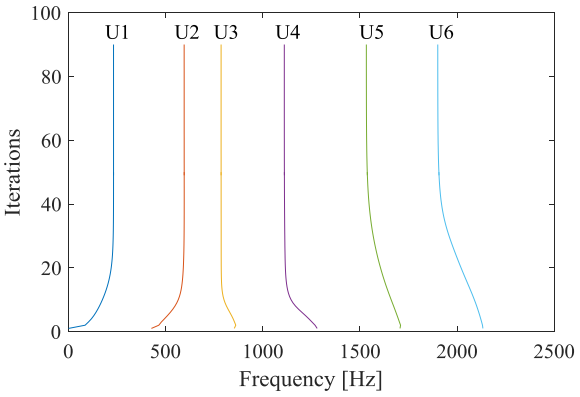

FIGURE 27. The number of iterations of modal center frequencies.

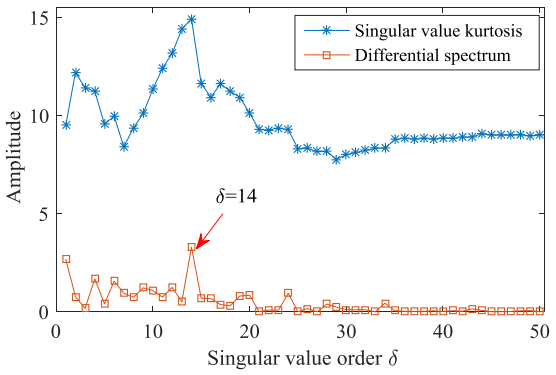

FIGURE 28. Singular kurtosis difference spectrum of the U5 sensitive component.

kurtosis difference spectrum are given in Fig. 28. It can be seen from Fig. 28 that the reconstructed order is chosen to be 14. Thus, the first fourteen singular values are selected for signal reconstruction, and the reconstructed signal is shown in Fig. 29(a). It can be observed that a regular impact component clearly appears in the reconstructed signal.

Fig. 29(b) shows the envelope spectrum of the reconstructed signal. It can be seen from Fig. 29(b) that the three times of the planetary gear fault characteristic frequency $3f_p$ and its sixth harmonic $6f_p$ are dominant, and the remainder peaks mainly appear in the planetary gear fault characteristic frequency f_p and its harmonics nf_p, the planet carrier rotating frequency f_c and its harmonics mf_c, and their sum and difference combination with the planetary gear characteristic frequency and its harmonics $nf_p \pm mf_c(m, n = 1, 2...)$. (These phenomena indicate that the planetary gear fault causes the load distribution between the planetary gears to be uneven, which enlarges the amplitude modulation effect of the planet carrier on the meshing vibration. In addition, the transmission path of the fault vibration changes with the rotation of the planetary carrier, and it also has an amplitude modulation effect on the planetary gear fault vibration. These factors lead to the planetary gear fault characteristic frequency and its harmonics, the planet carrier rotating frequency and its harmonics, as well as their sum and difference combination with the planetary gear characteristic frequency and its harmonics

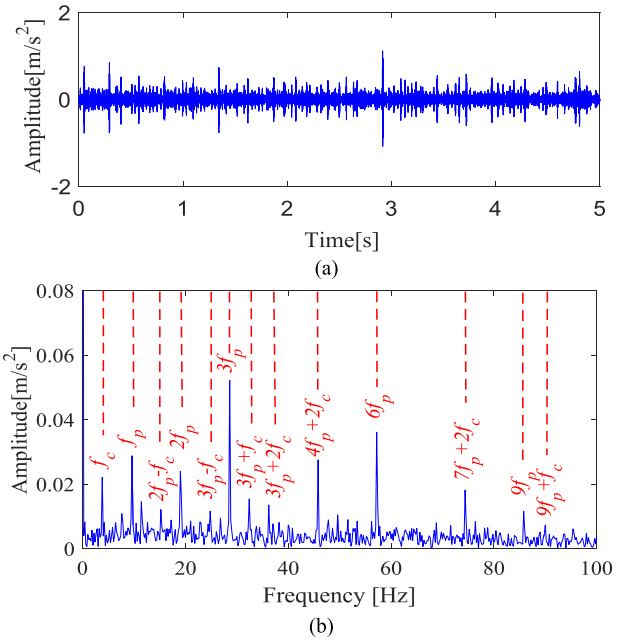

FIGURE 29. The processing result of sun gear fault signal by the proposed method: (a) The reconstructed signal obtained by the proposed method, (b) The envelope spectrum of the reconstructed signal.

in the envelope spectrum.) These features imply that a local fault has occurred in the planetary gear, which is consistent with the actual experimental setting.

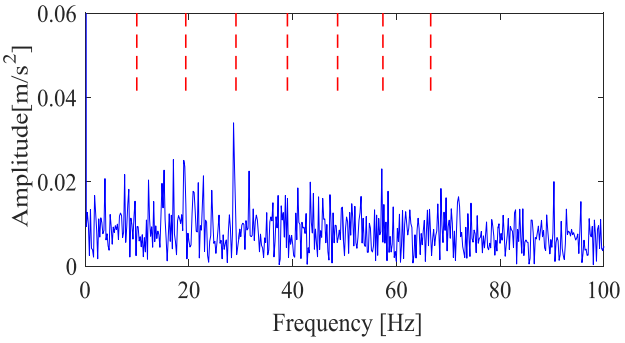

FIGURE 30. Direct envelope analysis of U5 modal component.

For comparison, the direct envelope demodulation analysis is performed on the U5 component obtained by the APOVMD method, as shown in Fig. 30. It can be seen that there are peaks at the three times of the planetary gear fault characteristic frequency and harmonics, but other unrelated frequency peaks is also abundant, which causes serious interference to extract the fault feature information.

The VMD-SVD method is applied to analyze the same planetary gear fault signal shown in Fig. 31. From the reconstructed signal of Fig. 31(a), the impact features cannot be extracted visibly, while from the envelope spectrum of Fig. 31(b), although there are peaks at the three times of the planetary fault characteristic frequency $3f_p$ and its second harmonic $6f_p$, other irrelevant frequencies also have

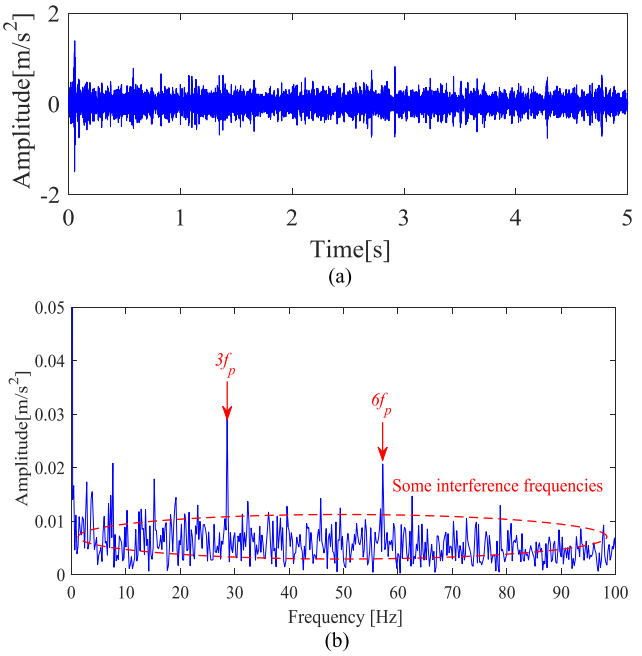

FIGURE 31. Comparative analysis of planetary gear fault signal processed by VMD-SVD method: (a) The reconstructed signal obtained by VMD-SVD method, (b) The envelope spectrum of the reconstructed signal.

stronger energy, and the analysis result is not good as shown in Fig. 29(b).

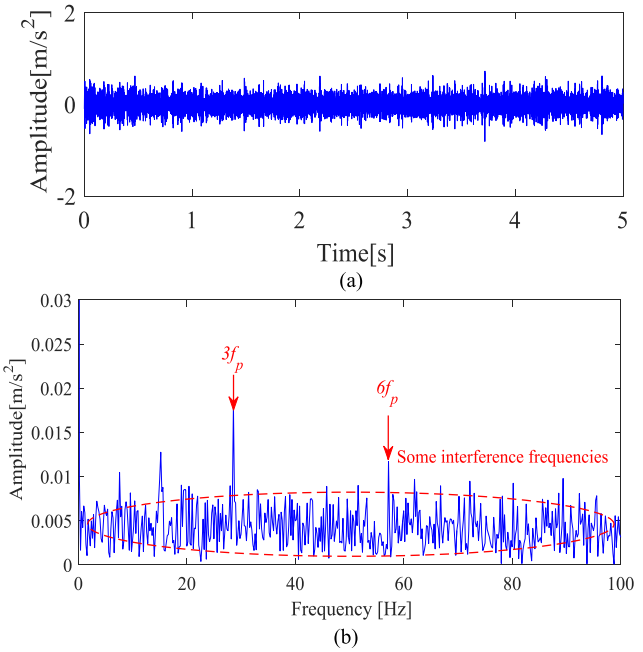

FIGURE 32. Comparative analysis of planetary gear fault signal processed by EEMD-SVD method: (a) The reconstructed signal obtained by EEMD-SVD method, (b) The envelope spectrum of the reconstructed signal.

The EEMD-SVD method is used to process the same planetary gear fault signal shown in Fig. 32. From the

reconstructed signal of Fig. 32(a), no obvious periodic fault impact feature can be observed. Moreover, in the envelope spectrum of Fig. 32(b), the envelope spectrum characteristics are similar to those in Fig. 31(b), and the interference of the noise frequency is still serious. Compared with Fig. 29(b), this method can not clearly extract the fault characteristics.

VI. CONCLUSION

In this study, an early weak fault feature extraction method based on APOVMD and singular kurtosis difference spectrum is proposed, and successfully applied to planetary gearbox fault diagnosis. APOVMD adaptively chooses the modal number and penalty factor by the ratio of central frequency of modal component, which not only solves the problem that the decomposition parameters in the original VMD cannot be effectively determined, but also overcomes the possible information loss problem or over-decomposition problem of VMD. The cosine similarity index is used to select the modal that contains abundant fault feature information from the decomposed modal component of APOVMD as the sensitive component, which is a effective fault information selection criteria and reduces the blindness of component selection. However, because the early fault signal of planetary gearbox is weak and easily submerged by strong noise, the single APOVMD method is not ideal. So it is combined with the singular kurtosis differential spectrum to achieve early fault diagnosis of planetary gearbox. The singular kurtosis differential spectrum method effectively solves the problem that the reconstruction order cannot be accurately determined in SVD. This method makes full use of the sensitivity of kurtosis to impact signals, which has a solid theoretical foundation, and it is easy to understand by users. To demonstrate the feasibility and superiority of the proposed method, compare with the VMD-SVD and EEMD-SVD methods. As a result, the proposed method can more clearly and effectively extract the planetary gearbox fault characteristic frequency and its harmonic characteristics. In future research, the performance of the proposed method will be investigated under variable speed operating conditions.

ACKNOWLEDGMENT

The authors would like to thank the anonymous reviewers for their valuable comments and help to improve this manuscript.

REFERENCES

[1] L. Liu, X. Liang, and M. J. Zuo, "A dependence-based feature vector and its application on planetary gearbox fault classification," *J. Sound Vib.*, vol. 431, pp. 192–211, Sep. 2018.

[2] X. Jiang and S. Li, "A dual path optimization ridge estimation method for condition monitoring of planetary gearbox under varying-speed operation," *Measurement*, vol. 94, pp. 630–644, Dec. 2016.

[3] X.-H. Chen *et al.*, "Research of weak fault feature information extraction of planetary gear based on ensemble empirical mode decomposition and adaptive stochastic resonance," *Measurement*, vol. 73, pp. 55–67, Sep. 2015.

[4] Y. Li, K. Ding, G. He, and X. Jiao, "Non-stationary vibration feature extraction method based on sparse decomposition and order tracking for gearbox fault diagnosis," *Measurement*, vol. 124, pp. 453–469, Aug. 2018.

[5] Y. Lei, Y. Liu, J. Lin, and F. Lu, "Phenomenological models of vibration signals for condition monitoring and fault diagnosis of epicyclic gearboxes," *J. Sound Vib.*, vol. 369, pp. 28–266, May 2016.

[6] M. Zhang, K. Wang, D. Wei, and M. J. Zuo, "Amplitudes of characteristic frequencies for fault diagnosis of planetary gearbox," *J. Sound Vib.*, vol. 432, pp. 119–132, Oct. 2018.

[7] B. Tang, W. Liu, and T. Song, "Wind turbine fault diagnosis based on Morlet wavelet transformation and Wigner-Ville distribution," *Renew. Energy*, vol. 35, no. 12, pp. 2862–2866, Dec. 2010.

[8] V. Dekys, P. Kalman, P. Hanak, P. Novak, and Z. Stankovicova, "Determination of vibration sources by using STFT," *Procedia Eng.*, vol. 177, pp. 496–501, Jan. 2017.

[9] N. Saravanan and K. I. Ramachandran, "Incipient gear box fault diagnosis using discrete wavelet transform (DWT) for feature extraction and classification using artificial neural network (ANN)," *Expert Syst. Appl.*, vol. 37, no. 6, pp. 4168–4181, Jun. 2010.

[10] Y. Lei, J. Lin, Z. He, and M. J. Zuo, "A review on empirical mode decomposition in fault diagnosis of rotating machinery," *Mech. Syst. Signal Process.*, vol. 35, nos. 1–2, pp. 108–126, Feb. 2013.

[11] Z. Shen, X. Chen, X. Zhang, and Z. He, "A novel intelligent gear fault diagnosis model based on EMD and multi-class TSVM," *Measurement*, vol. 45, pp. 30–40, Jan. 2012.

[12] C. Junsheng, Y. Dejie, and Y. Yu, "The application of energy operator demodulation approach based on EMD in machinery fault diagnosis," *Mech. Syst. Signal Process.*, vol. 21, no. 2, pp. 668–677, Feb. 2007.

[13] J. S. Smith, "The local mean decomposition and its application to EEG perception data," *J. Roy. Soc. Interface*, vol. 2, no. 5, pp. 443–454, 2005.

[14] Z. Wu and N. E. Huang, "Ensemble empirical mode decomposition: A noise-assisted data analysis method," *Adv. Adapt. Data Anal.*, vol. 1, no. 1, pp. 1–41, 2009.

[15] Y. Yang, J. Cheng, and K. Zhang, "An ensemble local means decomposition method and its application to local rub-impact fault diagnosis of the rotor systems," *Measurement*, vol. 45, no. 3, pp. 561–570, Apr. 2012.

[16] L. Wang, Z. Liu, Q. Miao, and X. Zhang, "Complete ensemble local mean decomposition with adaptive noise and its application to fault diagnosis for rolling bearings," *Mech. Syst. Signal Process.*, vol. 106, pp. 24–39, Jun. 2018.

[17] K. Dragomiretskiy and D. Zosso, "Variational mode decomposition," *IEEE Trans. Signal Process.*, vol. 62, no. 3, pp. 531–544, Feb. 2014.

[18] Y. Li, G. Cheng, C. Liu, and X. Chen, "Study on planetary gear fault diagnosis based on variational mode decomposition and deep neural Networks," *Measurement*, vol. 130, pp. 94–104, Dec. 2018.

[19] Y. Li, G. Li, Y. Wei, B. Liu, and X. Liang, "Health condition identification of planetary gearboxes based on variational mode decomposition and generalized composite multi-scale symbolic dynamic entropy," *ISA Trans.*, vol. 81, pp. 329–341, Oct. 2018.

[20] F. Li, R. Li, L. Tian, L. Chen, and J. Liu, "Data-driven time-frequency analysis method based on variational mode decomposition and its application to gear fault diagnosis in variable working conditions," *Mech. Syst. Signal Process.*, vol. 116, pp. 462–479, Feb. 2019.

[21] M. Zhang, Z. Jiang, and K. Feng, "Research on variational mode decomposition in rolling bearings fault diagnosis of the multistage centrifugal pump," *Mech. Syst. Signal Process.*, vol. 93, pp. 460–493, Sep. 2017.

[22] A. Upadhyay, M. Sharma, and R. B. Pachori, "Determination of instantaneous fundamental frequency of speech signals using variational mode decomposition," *Comput. Elect. Eng.*, vol. 62, pp. 630–647, Aug. 2017.

[23] J. Li, W. Tang, J. Wang, and X. Zhang, "Multilevel thresholding selection based on variational mode decomposition for image segmentation," *Signal Process.*, vol. 147, pp. 80–91, Jun. 2018.

[24] R. Golafshan and K. Y. Sanliturk, "SVD and Hankel matrix based denoising approach for ball bearing fault detection and its assessment using artificial faults," *Mech. Syst. Signal Process.*, vols. 70–71, pp. 36–50, Mar. 2016.

[25] H. Jiang, J. Chen, G. Dong, T. Liu, and G. Chen, "Study on Hankel matrix-based SVD and its application in rolling element bearing fault diagnosis," *Mech. Syst. Signal Process.*, vols. 52–53, pp. 338–359, Feb. 2015.

[26] K. Yu, T. Lin, and J. Tan, "A bearing fault diagnosis technique based on singular values of EEMD spatial condition matrix and Gath-Geva clustering," *Appl. Acoust.*, vol. 121, pp. 33–45, Jun. 2017.

[27] Z. Liao, L. Song, P. Chen, Z. Guan, Z. Fang, and K. Li, "An effective singular value selection and bearing fault signal filtering diagnosis method based on false nearest neighbors and statistical information criteria," *Sensors*, vol. 18, no. 7, pp. 2235–2247, Jul. 2018.

[28] M. Zhao and X. Jia, "A novel strategy for signal denoising using reweighted SVD and its applications to weak fault feature enhancement of rotating machinery," *Mech. Syst. Signal Process.*, vol. 94, pp. 129–147, Sep. 2017.
[29] X. Zhao and B. Ye, "Selection of effective singular values using difference spectrum and its application to fault diagnosis of headstock," *Mech. Syst. Signal Process.*, vol. 25, no. 5, pp. 1617–1631, 2011.
[30] H. Zhao, S. Guo, and D. Gao, "Fault feature extraction of bearing faults based on singular value decomposition and variational modal decomposition," *J. Vib. Shock*, vol. 35, no. 22, pp. 183–188, Nov. 2016.
[31] J. Ding, J. Lin, and J. Zhao, "Detection of the dynamic imbalance with cardan shaft in high-speed train applying EEMD-Hankel-SVD," *China J. Mech. Eng.*, vol. 51, no. 10, pp. 143–151, Jan. 2015.
[32] S. Tong, Y. Zhang, J. Xu, and F. Cong, "Pattern recognition of rolling bearing fault under multiple conditions based on ensemble empirical mode decomposition and singular value decomposition," *Proc. Inst. Mech. Eng., Part C, J. Mech. Eng. Sci.*, vol. 232, no. 12, pp. 2280–2296, May 2017.
[33] H. Kalhori, M. M. Alamdari, and L. Ye, "Automated algorithm for impact force identification using cosine similarity searching," *Measurement*, vol. 122, pp. 648–657, Jul. 2018.
[34] E. P. Chou and S. M. Hsu, "Cosine similarity as a sample size-free measure to quantify phase clustering within a single neurophysiological signal," *J. Neurosci. Meth.*, vol. 295, pp. 111–120, Feb. 2018.
[35] J. Antoni and R. Randall, "The spectral kurtosis: Application to the vibratory surveillance and diagnostics of rotating machines," *Mech. Syst. Signal Process.*, vol. 20, no. 2, pp. 308–331, 2006.
[36] J. Obuchowski, R. Zimroz, and A. Wyłoma ska, "Blind equalization using combined skewness–kurtosis criterion for gearbox vibration enhancement," *Measurement*, vol. 88, pp. 34–44, Jun. 2016.
[37] Z. Feng and M. J. Zuo, "Vibration signal models for fault diagnosis of planetary gearboxes," *J. Sound Vib.*, vol. 331, no. 22, pp. 4919–4939, 2012.
[38] Z. Feng, X. Lin, and M. J. Zuo, "Joint amplitude and frequency demodulation analysis based on intrinsic time-scale decomposition for planetary gearbox fault diagnosis," *Mech. Syst. Signal Process.*, vol. 72, pp. 223–240, May 2016.

CHAOGE WANG (S'–) received the B.Sc. degree in mechanical engineering and automation from Shenyang Aerospace University, China, in 2014, and the M.Sc. degree in machinery manufacturing and automation from the Inner Mongolia University of Science and Technology, China, in 2017. He is currently pursuing the Ph.D. degree in mechanical and electronic engineering with the Dalian University of Technology, China. His research interests include rotating machinery fault diagnosis and signal processing. His awards and honors include the National Scholarship, the Master's Excellent Graduates Award from the Inner Mongolia University of Science and Technology, and the Excellent Graduate Award from the Dalian University of Technology.

HONGKUN LI received the B.Sc. degree in internal combustion engine engineering and the Ph.D. degree in mechanical design and theory from the Dalian University of Technology, China, in 1997 and 2003, respectively. From 2003 to 2005, he was a Postdoctoral Research Fellow with the Department of Mechanical Engineering, University of Strathclyde, U.K. He is currently a Professor with the School of Mechanical Engineering, Dalian University of Technology. He has been responsible for the research work of the National Natural Science Foundation of China and the Major Sub-Projects of National Science and Technology. He has participated in the research work of the National Science and Technology Support Plan, 973, and 863 Projects. He has published more than 100 academic papers in conferences and respectable journals. His research interests include fault diagnosis and operation reliability assessment, weak signal feature information extraction, artificial intelligence, and vibration and noise control. He was a recipient of the China Machinery Industry Federation First Prize and the China Machinery Industry Science and Technology Award.

GANGJIN HUANG received the B.S. degree in electrical engineering and automation from the Mianyang Teachers' College, China, in 2015, and the M.S. degree in instrumentation engineering from the Kunming University of Science and Technology, China, in 2018. He is currently pursuing the Ph.D. degree in machinery manufacturing and automatization with the Dalian University of Technology, China. His research interests include mechanical weak signal feature information extraction methods, fault diagnosis and operational reliability assessment, and prediction of mechanical remaining life. His awards and honors include the Master's National Scholarship and the Wu Daguan Scholarship from the Kunming University of Science and Technology.

JIAYU OU received the B.S. degree in mechanical design and manufacturing and automation from the University of Science and Technology Liaoning, China, in 2017. She is currently pursuing the M.Sc. and Ph.D. degrees in machinery manufacturing and automatization with the Dalian University of Technology, China. Her research interests include milling tool wear feature information extraction methods, fault diagnosis, and prediction of tool remaining life. Her awards and honors include the Excellent Graduates Award for Undergraduates and National Motivation Scholarship for College Students from the University of Science and Technology Liaoning.